Gigacycle fatigue data sheets for advanced engineering materials

Available online at www.sciencedirect.com
ScienceDirect
Science and Technology of Advanced Materials 8 (2007) 545–551
SCIENCE AND TECHNOLOGY OF ADVANCED MATERIALS
www.elsevier.com/locate/stam

Review

Gigacycle fatigue data sheets for advanced engineering materials

Koji Yamaguchi*, Takayuki Abe, Kazuo Kobayashi, Etsuo Takeuchi, Hisashi Hirukawa, Yoshio Maeda, Nobuo Nagashima, Masao Hayakawa, Yoshiyuki Furuya, Masuo Shimodaira, Kensuke Miyahara

Fatigue group, Materials Reliability Center, National Institute for Materials Science, 1-2-1, Sengen, Tsukuba, Ibaraki 305-0047, Japan

Received 31 August 2007; received in revised form 28 September 2007; accepted 28 September 2007
Available online 19 November 2007

Abstract

Gigacycle fatigue data sheets have been published since 1997 by the National Institute for Materials Science. They cover several areas such as high-cycle-number fatigue for high-strength steels and titanium alloys, the fatigue of welded joints, and high-temperature fatigue for advanced ferritic heat-resistant steels. Some unique testing machines are used to run the tests up to an extremely high number of cycles such as 10^{10} cycles. A characteristic of gigacycle fatigue failure is that it is initiated inside smooth specimens; the fatigue strength decreases with increasing cycle number and the fatigue limit disappears, although ordinary fatigue failure initiates from the surface of a smooth specimen and a fatigue limit appears. For welded joints, fatigue failure initiates from the notch root of the weld, because a large amount of stress is concentrated at the weld toe. The fatigue strength of welded joints has been obtained for up to 10^8 cycles, which is an extremely high number of cycles for large welded joints. The project of producing gigacycle fatigue data sheets is still continuing and will take a few more years to complete.

Keywords: Gigacycle fatigue; Interior fracture; High-strength steels; Titanium alloys; Fatigue strength; Welded joints; High-temperature fatigue; Heat-resistant steels

Contents

1. Introduction

The National Institute for Materials Science (NIMS), and before that, the National Research Institute for Metals (NRIM), has published the fatigue data sheets since 1975. At that time, there were no reliable fatigue strength data for engineering materials. In designing a machine or structure subjected to repeated loading, it was necessary to collect the data of the fatigue strength of the materials from the literature. However, the data had a broad scatter band because the experimental test conditions including specimen size, type of testing machine, frequency of the repeated load, and applied load condition, were varied considerably among the laboratories.

*Corresponding author.
E-mail address: YAMAGUCHI.Koji@nims.go.jp (K. Yamaguchi).

1468-6996/$ - see front matter © 2007 Published by Elsevier Ltd.
doi:10.1016/j.stam.2007.09.009

To obtain reliable and standard fatigue strength data for Japanese fundamental engineering materials, a national project was started at NIMS in 1975 [1]. An advisory committee was also established at NIMS to determine the most effective direction of this project. The committee recommended that NIMS should take responsibility for everything from the selection of materials and the preparation of specimens to the fatigue tests and the analysis of the data [1].

Systematic results with less scatter were published as NIMS fatigue data sheets and technical documents for about 20 years from 1975. Eighty-four volumes of data sheets [2] and 17 technical documents [3] for about 50 types of fundamental engineering materials were published. The initial purpose of this project was achieved and the project was completed in 1995.

An example of one of the above data sheets is shown in Fig. 1 [4], in which the results of 11 types of fundamental JIS standard steel such as carbon and low-alloy steels are shown. For each steel, nine steel blocks were prepared and three samples subject to different heat treatments were cut from each steel block; thus, the data for each steel were accumulated from a total of 27 samples. The specimens were smooth cylindrical bars with a diameter of 8 mm for all the materials. The fatigue tests were performed by rotating bending, and the frequency was 30 Hz. This figure shows a clear correlation between the fatigue limit at 10^7 cycles, σ_{wb}, and the tensile strength, σ_B, for the materials, expressed by the following equation:

$$\sigma_{wb} \fallingdotseq 0.5\sigma_B. \quad (1)$$

This relationship is widely accepted as a useful empirical equation. This was one of the outcomes resulting from the first stage of compiling fatigue data sheets.

Recently, the fatigue properties of materials for very high cycle numbers of over 10^7 cycles have been studied with keen interest. The numbers of high-speed machines and highly efficient structures are increasing, and high-strength materials are being used increasingly in applications such as the springs and axles of automobiles or high-speed trains, tall buildings, bridges, the turbo engines of rockets, and high-efficiency supercritical power plants. Some high-strength materials and advanced new materials fail after over 10^7 cycles.

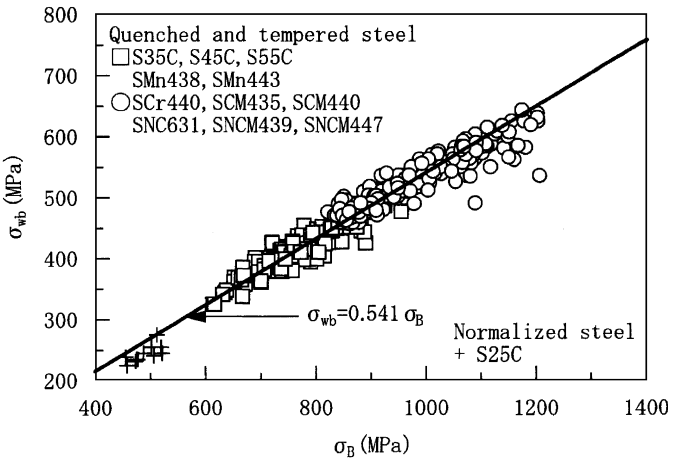

Fig. 1. Relationship between rotating bending fatigue strength at 10^7 cycles and the tensile strength for various types of engineering material.

In conventional fatigue tests, the fatigue limit is determined at 10^7 cycles, and fatigue cracks tend to initiate from the specimen surface. On the other hand, for very high cycle numbers over 10^7 cycles, the failure is initiated from nonmetallic inclusions, microstructure defects, or transgranular facets inside the specimen [5]. This is important because the fatigue strength decreases significantly with increasing number of cycles, and the fatigue limit disappears. This means that safe-life design technique is not valid and the safety margin should be increased or a fail-safe design should be applied.

A new project to produce long-term fatigue data sheets for advanced materials for very high cycle numbers of over 10^7 cycles was started in 1997 [6]. Such fatigue behavior was named gigacycle fatigue by NIMS [7]. Gigacycle fatigue means that the failure is initiated not from the surface but from the interior of the specimen.

In this paper, new testing machines and the results from gigacycle fatigue data sheets are introduced.

2. Gigacycle fatigue for high-strength steels and titanium alloys

It takes a long time to run gigacycle fatigue tests. For example, it takes about 3 years to run a test of 10^{10} cycles at 100 Hz. One method of obtaining the long-term data is, thus, to run continuous tests for 3 years. Another method is to use very-high-frequency testing machines.

Figs. 2 and 3 show the testing machines used for gigacycle fatigue tests of up to 10^{10} cycles. Fig. 2 shows a multiple-axis, cantilever-type, rotating bending fatigue-testing machine [8,9], which is able to run 48 tests at the same time. The specimen diameter is also 8 mm and the frequency is 100 Hz. This machine is suitable for continuous long-term tests, because it is almost maintenance-free. On the other hand, Fig. 3 shows an ultrasonic high-frequency fatigue-testing machine [10,11] equipped with a piezoactuator. The loading condition is the push–pull type. The frequency is an ultrasonic 20 kHz and the specimen diameter is 3 mm.

Figs. 4 and 5 show the fatigue-test results for a high-strength spring steel SUP 7 tempered at 430 °C obtained using the rotating bending [7] and ultrasonic machines [12], respectively. These results show that the type of applied load, rotating bending or push–pull, and the size of the specimens have no effect on the results. Moreover, there is no frequency effect between 30 Hz and 20 kHz. Even in the ultrasonic-frequency tests, the temperature of the specimen does not increase under air-cooled conditions because the applied stress is very small. The data obtained from the 20 kHz machine are coincident with the conventionally obtained data in Fig. 4. The fish-eye failure mode occurs

Fig. 2. Multiple-axis, cantilever-type rotating bending machine for testing gigacycle fatigue.

Fig. 3. Ultrasonic high-frequency machine for testing gigacycle fatigue.

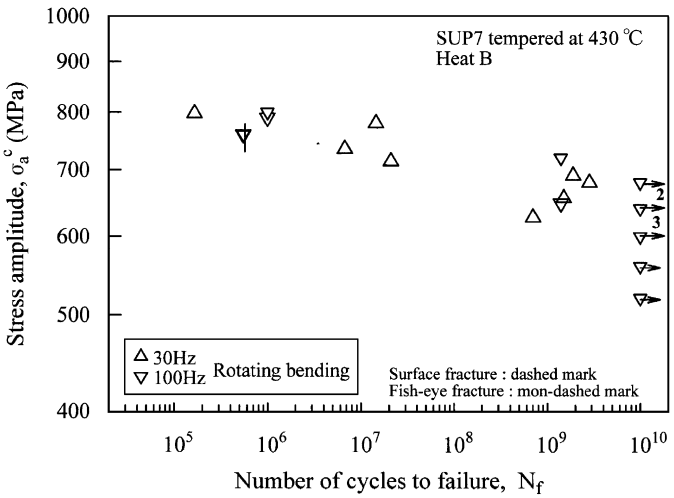

Fig. 4. Rotating bending fatigue strength of SUP 7 spring steel.

for almost all the specimens. A typical fracture surface is shown in Fig. 6 [11]. The initiation site of the fracture is a nonmetallic inclusion such as Al_2O_3.

The results of fatigue tests for a titanium alloy are shown in Fig. 7 [13]. The testing machines used are an electromagnetic-resonance-type machine with a frequency of 120 Hz and the 20 kHz ultrasonic machine. The specimen diameter of the electromagnetic resonance-type machine is 6 mm. Both load conditions are push–pull type. A marked decrease in fatigue strength is observed over 10^7 cycles for the titanium alloy. However, in this case, the failure mode is interior but there are no inclusions at the initiation site of the fracture surface. Fig. 8 shows the fracture surface of Ti-6Al-4V alloy in the gigacycle fatigue region [13]. The initiation site may be a microstructure defect on the boundary. In the case of low-temperature fatigue or

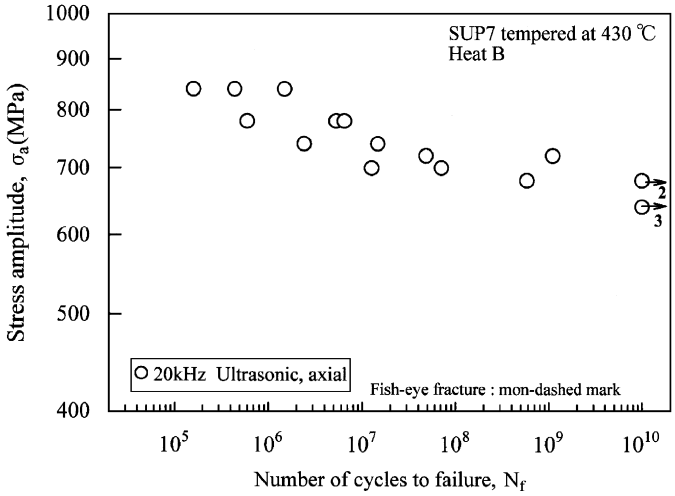

Fig. 5. Ultrasonic (push–pull type) fatigue strength of SUP 7 spring steel.

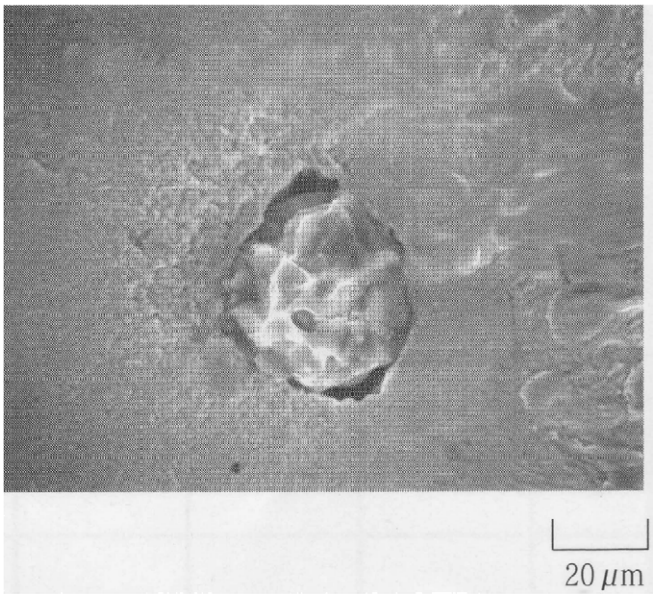

Fig. 6. Initiation site of high-cycle-number fatigue. Al_2O_3 on the fracture surface of SUP 7 spring steel.

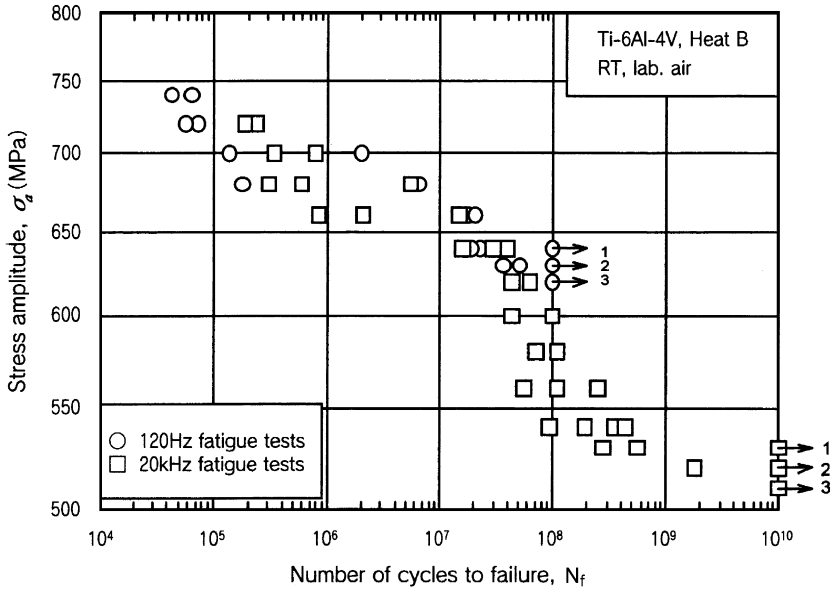

Fig. 7. Push–pull-type fatigue strength of titanium alloy at frequencies of 120 and 20 kHz.

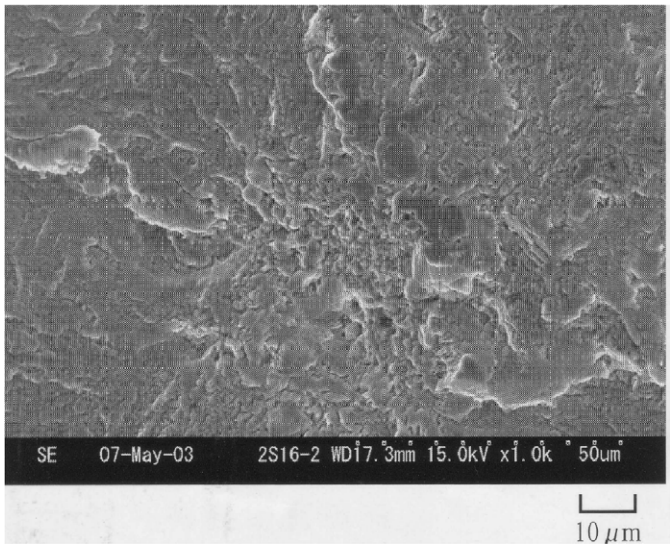

Fig. 8. Fracture surface of titanium alloy. The fracture mode is interior, but there are no nonmetallic inclusions.

coarse-grained forged titanium alloys, clear crystallographic facets are observed at the fracture surface, which are the initiation sites of fatigue fracture [14].

The effect of hydrogen on gigacycle fatigue failure for high-strength steels is now being focused on. At NIMS these effects are also now being investigated for hydrogen-charged steels [15].

3. Fatigue strength of welded joints

The fatigue strength of welded joints is generally considered to be affected by the weld residual stress and the stress concentration at the weld toe [16]. Usually the residual stress at the weld toe is tensional; thus, the fatigue strength of the welded joints decreases [17]. Also, the stress concentration factor at the weld toe is usually large. The factor is about 2–3 for butt-welded joints and 3–10 for cruciform-welded joints, depending on factors such as the weld toe radius and plate thickness. The effects of the residual stress and the stress concentration at the weld toe have not yet been distinguished clearly [18].

In this series, the effect of plate thickness and plate width is under investigation by systematically varying those of specimens. Fig. 9 shows the specimen profiles used to investigate the effect of plate thickness between 9 and 160 mm. The welded joints here are non-load-carrying cruciform-welded joints.

An example of fatigue-test results for the welded joints is shown in Fig. 10 [19–21]. This figure shows the effect of plate thickness on the fatigue strength of the cruciform-welded joints. The test is under zero tension so that the stress ratio, $R = \sigma_{min}/\sigma_{max}$, is zero and the frequency is 5–50 Hz. In Fig. 10, the fatigue strength decreases over 10^7 cycles and the fatigue limit first appears at 10^8 cycles.

Fig. 11 shows the relationship between K_f and K_t, where K_f is the notch factor derived from $\sigma_{\text{base metal}}/\sigma_{\text{welded joints}}$, and K_t is the stress concentration factor at the weld toe. $\sigma_{\text{base metal}}$ and $\sigma_{\text{welded joints}}$ are the fatigue strengths at 10^8 cycles for the base metal and welded joints, respectively. In this study it is unusual to obtain a fatigue strength at 10^8 cycles even for large specimens. The fatigue strength of welded joints may be mainly determined by the stress concentration factor K_t.

Usually the notch effect for a small round-cylindrical specimen of base metal saturates at $K_t = 2$ or 3, as shown by the dotted line in Fig. 11, because a nonpropagating crack appears at the notch root. In other words, the fatigue limit does not decrease with K_t over $K_t = 2$ or 3. This is generally considered to be due to plasticity-induced crack

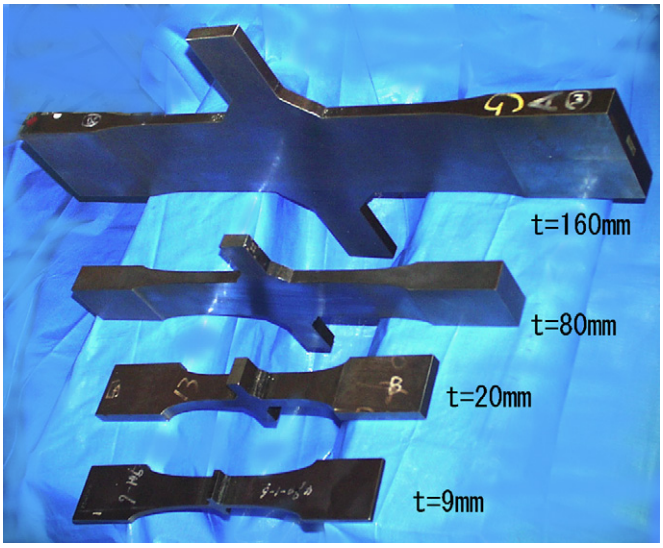

Fig. 9. Specimens of non-load-carrying cruciform-welded joints. t is the plate thickness.

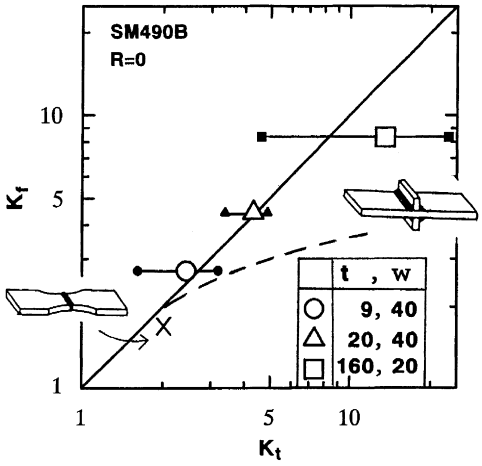

Fig. 11. Relationship between notch factor K_f and stress concentration factor K_t. The dotted line indicates the behavior of the notch specimen without residual stress, like a machined round-bar notch specimen. X indicates the data for butt-welded joints [21].

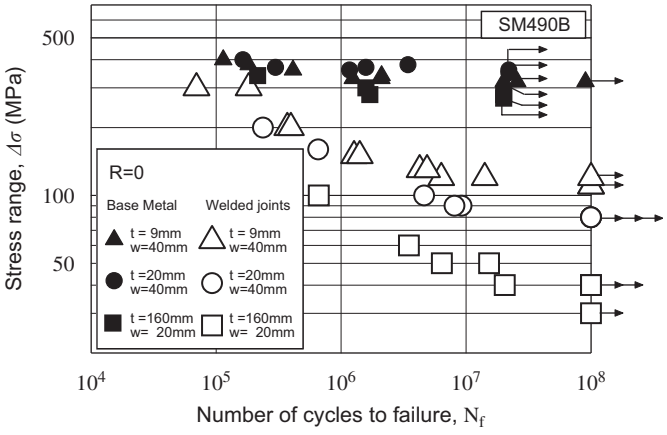

Fig. 10. Effect of plate thickness on the fatigue strength of cruciform-welded joints. t is the thickness and w is the width of the plate.

closure, oxide-induced crack closure, or roughness-induced crack closure at the tip of the crack [5]. On the other hand, the notch effect K_f for welded joints does not saturate over $K_t = 2$ or 3 because it is thought that the tensional residual stress at the weld toe results in the propagation of a fatigue crack initiated at the weld toe. The data for butt-welded joints, which were obtained 20 years ago [22], are also indicated in Fig. 11. The concentration factor for butt-welded joints is small; thus, the effects of stress concentration and residual stress were not distinguished clearly.

It is difficult to quantitatively measure the residual stress immediately below the weld toe. However, it is necessary to recognize that some tensional residual stress always exists at the weld toe, which may induce the propagation of cracks.

4. High-temperature fatigue

High chromium ferritic steels for use in supercritical power plants operating at 625–650 °C have been developed in Japan in place of austenitic stainless steels [23]. The steels are 9% Cr–2% W and 12% Cr–2% W for high-efficiency power plants [23] in Japan as well as modified 9% Cr–1% Mo steel. In high-temperature fatigue data sheets, the results for long-term-fatigue and creep-fatigue tests on these advanced steels are reported.

For high-temperature gigacycle fatigue tests, a servo-hydraulic fatigue machine with a frequency of 1 kHz is used, as shown in Fig. 12. This machine has a servo-valve of voice coil type for high frequency. Induction heating is used for high-temperature tests [24] and the specimen diameter is 3 mm. For creep-fatigue tests, axial-strain-controlled, digitalized conventional hydraulic machines are used. In this case, the specimen diameter is 10 mm.

The gigacycle fatigue properties for 12Cr–2W steel are shown in Fig. 13 [24]. The fatigue stress normalized by tensile strength σ_a/σ_B is used in the vertical axis in Fig. 13. The ratio at 10^9 cycles is about 0.5 at room temperature and 450 °C, but at 650 °C the ratio is below 0.5. Usually this ratio is about 0.5 for ordinary fatigue data, as shown in Fig. 1, but in the case of interior failure this ratio is below 0.5, such as at 650 °C for 12Cr–2W steel. At this temperature, the fracture surface is oxidized; however, interior fracture is observed for some specimens shown by dashes in Fig. 13 [24].

Examples of creep-fatigue data analysis by the strain-range partitioning method [25] are shown in Fig. 14 [26] and Fig. 15 [27] for ferritic and austenitic steels, respectively. The materials in Fig. 14 are ten types of ferritic steel used in supercritical power plants. The materials in Fig. 15 are low-carbon, medium-nitrogen 316FR austenitic steel and 20 types of 316FR steel modified by their production process, heat treatment, or chemical composition for use in fast-breeder reactors at 550 °C. The creep-fatigue tests were performed by applying a trapezoidal strain wave for a given tension hold time at

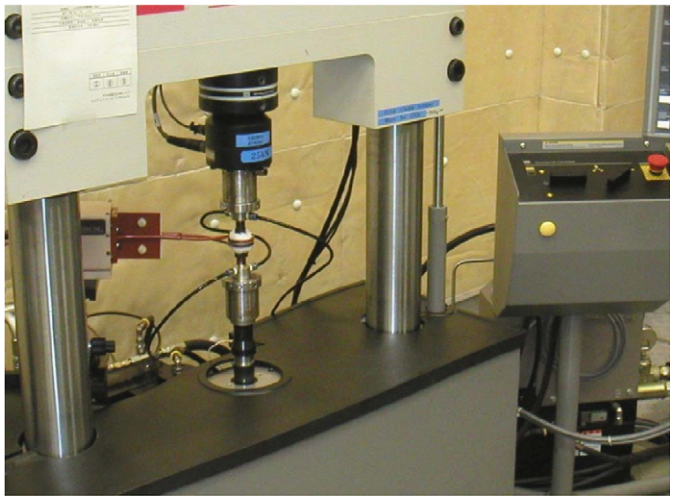

Fig. 12. 1 kHz servo-hydraulic machine for high-temperature fatigue testing. The temperature of the specimen is controlled by induction heating.

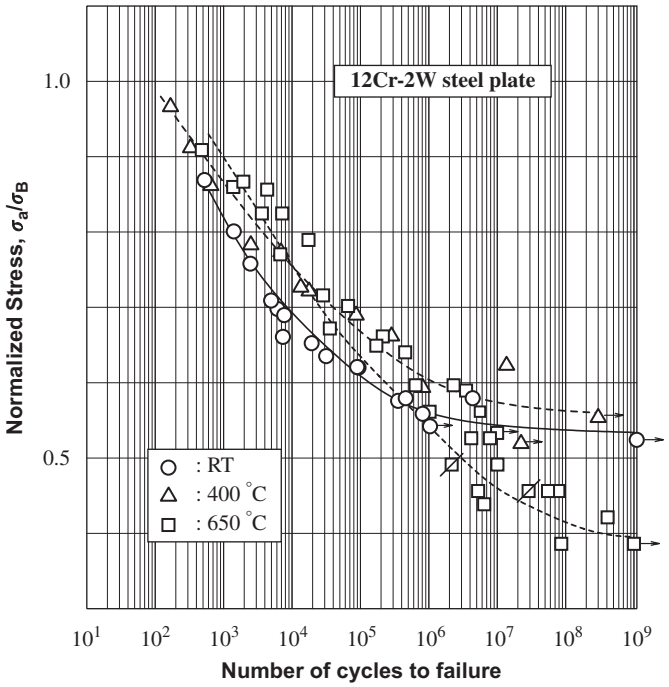

Fig. 13. Relationship between stress normalized by tensile strength and the number of cycles to failure for 12Cr–2W steel.

tension side. The testing temperatures are 650 and 550 °C for ferritic and austenitic steels, respectively.

The strain-range partitioning method can be used to describe the creep-fatigue data as follows using creep ductility:

$$\Delta\varepsilon_{cp}N_{cp}^{0.6} = 0.2D_c^{\alpha}. \quad (2)$$

This equation is applicable for both materials, where D_c is creep rupture ductility and α is 0.6 for ferritic steels and 2 for austenitic steel. $\Delta\varepsilon_{cp}$ and N_{cp} are the inelastic strain range and the number of cycles to failure, respectively, for

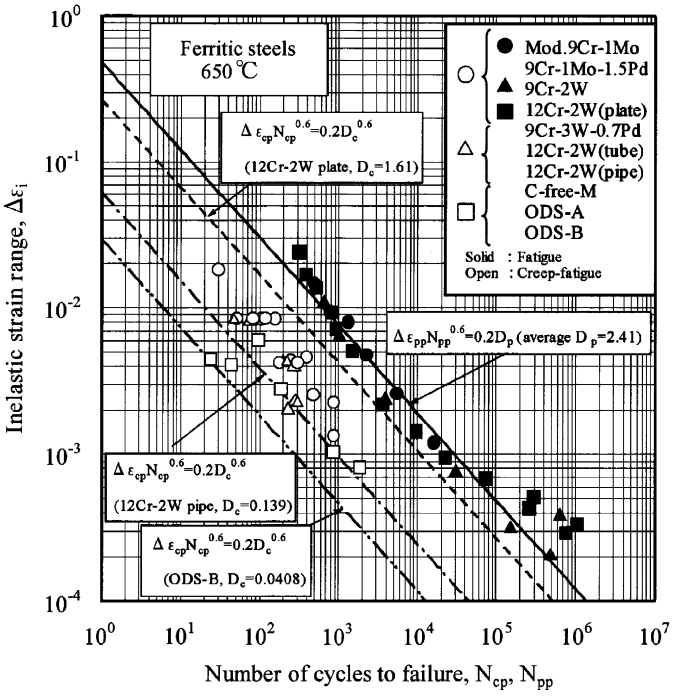

Fig. 14. Results obtained by strain-range partitioning method for ferritic steels.

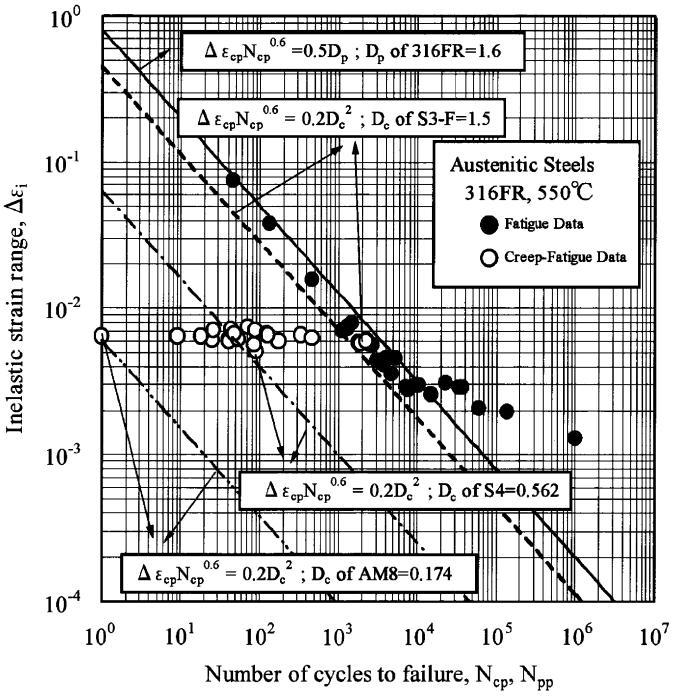

Fig. 15. Results obtained by strain-range partitioning method for austenitic stainless steels.

cp-type deformation, which is tensile creep deformation reversed by compressive plastic deformation. Therefore, $\Delta\varepsilon_{cp}$ and N_{cp} correspond to the inelastic strain range and the number of cycles to failure, respectively, for pure creep-fatigue conditions derived from the analysis of tension-hold-time test results. This analysis is based on the creep ductility and the strength of the materials throughout the

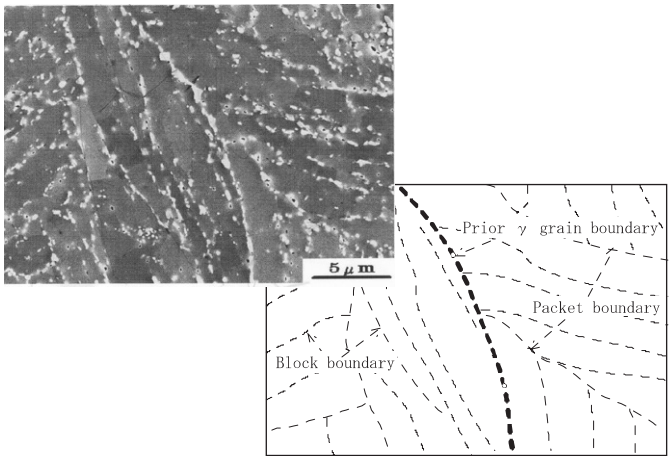

Fig. 16. Multiscale structure of ferritic steel observed by FE-SEM.

inelastic strain range, thus may be applicable for many types of material. The difference in materials is reflected by the index number α of creep ductility. Austenitic steels are more sensitive to creep ductility than ferritic steels.

The microstructures of advanced materials such as high-chromium ferritic steels have been investigated by a new observation method [28,29] in which the electrically polished surface is observed using a field-emission scanning electron microscope (FE-SEM) [30]. The result is shown in Fig. 16 [29]. The microstructure consists of prior austenitic (γ) grains, packets, and blocks. Lath boundaries exist inside the block domains. However, the lath boundaries are low-angle boundaries and are not observed by this method [30]. The lath structures can be observed using a transmission electron microscope [29]. These multiscale structures were first observed clearly for ferritic steel. This new observation method is applicable for the investigation of the mechanism of material strength, deformation, and microstructures. Observations by this method suggest that block boundaries play an important role in the strengthening mechanism and stable microstructure against the creep fatigue [28,29].

5. Conclusions

Gigacycle fatigue data sheets from No. 85 to No. 103 have been published since 1997. They consist of gigacycle fatigue data for high-strength steels and titanium alloys, the fatigue of welded joints, and high-temperature fatigue for advanced ferritic heat-resisting steels. Some unique testing machines are used for each of the fatigue tests, such as an ultrasonic fatigue-testing machine and a multiple-axis cantilever-type rotating bending fatigue-testing machine. Fatigue failure is initiated from the interior in gigacycle fatigue, and the fatigue strength of welded joints has been obtained for up to 10^8 cycles, which is an extremely high number of cycles for large welded joints. The project of producing gigacycle fatigue data sheets is still continuing and it will take a few more years to complete.

References

[1] NRIM Fatigue Data Sheet No. 0, 1978.
[2] NRIM Fatigue Data Sheets No. 1–No. 84 (1978–1994): these data sheets are available at 〈http://mits.nims.go.jp/〉.
[3] NRIM Materials Strength Data Sheet Technical Documents No. 1–No. 17, 1981–1997.
[4] NRIM Materials Strength Data Sheet Technical Document No. 5, 1989.
[5] Y. Murakami, Metal Fatigue: Effects of Small Defects and Nonmetallic Inclusions, Yokendo, Ltd., 1993.
[6] NRIM or NIMS Fatigue Data Sheets No. 85–No. 103, 2000–2007.
[7] NIMS Fatigue Data Sheet No. 87, 2002.
[8] Y. Furuya, S. Matsuoka, T. Abe, K. Yamaguchi, Scr. Mater. 46 (2002) 157.
[9] T. Abe, Y. Furuya, S. Matsuoka, Fatigue Frac. Eng. Mater. Struct. 27 (2004) 159.
[10] Y. Furuya, S. Matsuoka, T. Abe, Met. Trans. A 34A (2003) 2517.
[11] Y. Furuya, T. Abe, S. Matsuoka, Fatigue Frac. Eng. Mater. Struct. 26 (2003) 641.
[12] NIMS Fatigue Data Sheet No. 93, 2004.
[13] NIMS Fatigue Data Sheet No. 98, 2005.
[14] NIMS Space Use Materials Strength Data Sheet No. 1, 2003.
[15] H. Hirukawa, Y. Furuya, M. Hayakawa, Tetsu-to-Hagane 93 (2007) 36 (in Japanese).
[16] O. Watanabe, S. Matsumoto, Y. Nakano, Y. Saito, J. Jpn. Welding Soc. 13 (1995) 438.
[17] A. Ohta, Y. Maeda, N. Suzuki, J. Jpn. Welding Soc. 21 (2003) 603.
[18] A. Narumoto, S. Matsumoto, Y. Kawai, 19th Offshore Technology Conference, Houston, OTC, vol. 5558, 1987, p. 77.
[19] NIMS Fatigue Data Sheet No. 91, 2003.
[20] NIMS Fatigue Data Sheet No. 96, 2004.
[21] NIMS Fatigue Data Sheet No. 99, 2006.
[22] NRIM Materials Strength Data Sheet Technical Document No. 2, 1983.
[23] K. Kougami, H. Isaka, Tetsu-to-Hagane 76 (1990) 1043 (in Japanese).
[24] K. Kobayashi, K. Yamaguchi, M. Kimura, M. Hayakawa, J. Mater. Sci. 39 (2004) 6253.
[25] S.S. Manson, Fatigue at high temperatures, ASTM STP520, ASTM (1973) 599.
[26] M. Kimura, K. Kobayashi, K. Yamaguchi, Mater. Sci. Res. Int. 9 (2003) 50.
[27] M. Kimura, K. Kobayashi, K. Yamaguchi, JHPI 40 (2002) 262.
[28] M. Hayakawa, K. Yamaguchi, M. Kimura, K. Kobayashi, Mater. Trans. 45 (2004) 3291.
[29] M. Kimura, K. Yamaguchi, M. Hayakawa, K. Kobayashi, K. Kanazawa, Int. J. Fatigue 28 (2006) 300.
[30] M. Hayakawa, T. Hara, S. Matsuoka, K. Tsuzaki, J. Jpn. Inst. Met. 64 (2000) 460.